C. R. Physique 16 (2015) 193–203

Contents lists available at ScienceDirect

Comptes Rendus Physique

www.sciencedirect.com

Multiferroic materials and heterostructures / Matériaux et hétérostructures multiferroïques

Strain effects on multiferroic $BiFeO_3$ films

Effet de la déformation sur les films du matériau multiferroïque $BiFeO_3$

Yurong Yang [a,b,*], Ingrid C. Infante [c], Brahim Dkhil [c,*], Laurent Bellaiche [a,b]

[a] *Physics Department, University of Arkansas, 72701 Fayetteville, AR, USA*
[b] *Institute for Nanoscience and Engineering, University of Arkansas, 72701 Fayetteville, AR, USA*
[c] *Laboratoire "Structures, Propriétés et Modélisation des Solides", UMR 8580, CNRS & CentraleSupélec, Université Paris-Saclay, Grande Voie des vignes, 92295 Châtenay-Malabry cedex, France*

ARTICLE INFO

Article history:
Available online 14 February 2015

Keywords:
Multiferroics
$BiFeO_3$
Misfit strain
Thin film

Mots-clés :
Multiferroiques
$BiFeO_3$
Déformation
Adaptation de maille
Couche mince

ABSTRACT

The field of multiferroics has experienced a rapid progress resulting in the discovery of many new physical phenomena. $BiFeO_3$ (BFO) compound, which is one of the few room-temperature single-phase multiferroics, has contributed subsequently to this progress. As a result, significant review articles have been devoted specifically to this famous system. This chapter is dedicated to the strain effects on the structure stability and property changes of BFO thin films. It is a short and non-exhaustive topical overview that may be seen as an invitation for interested readers to go beyond. There is a very active and prolific research in this field and we apologize to the authors whose relevant work is not cited here. After a short introduction, we will thus review the effect of strain on BFO films by describing the consequences on the structure and the phase transitions as well as on polar, magnetic and magnetoelectric properties.

RÉSUMÉ

Le domaine des matériaux multiferroïques a connu un progrès rapide qui a permis la découverte de nombreux phénomènes physiques nouveaux. Le composé $BiFeO_3$ (BFO), qui est l'un des rares multiferroïques intrinsèques à température ambiante, a contribué à ce progrès de manière conséquente. Ainsi, des articles de revue ont déjà été consacrés spécifiquement à ce système moèle. Ici, cet article traite des effets de la déformation sur la stabilité structurale et sur les changements de propriétés dans le cas de films minces de BFO. Il s'agit d'un descriptif court et non exhaustif du sujet, qui peut se concevoir comme une invitation auprès des lecteurs intéressés à aller au delà. Du fait de la recherche très active et productive dans ce domaine, nous présentons par avance nos excuses aux auteurs dont les travaux ne sont pas cités ici. Après une courte introduction, nous allons ainsi passer en revue l'effet de la déformation sur les films de BFO, en décrivant les conséquences de cette dernière sur la structure et les transitions de phase ainsi que sur les propriétés polaires, magnétiques et magnétoélectriques.

* Corresponding authors.
E-mail addresses: yyrwater@uark.edu (Y. Yang), brahim.dkhil@centralesupelec.fr (B. Dkhil).

http://dx.doi.org/10.1016/j.crhy.2015.01.010
1631-0705/

1. Introduction

Multiferroics, also known as ferroelectromagnets, are materials possessing simultaneously two or more primary ferroic-like properties, such as electric polarization, elasticity, magnetization and/or toroidicity, within the same phase [1–5]. The richness of multiferroics arises from the cross-coupling between the present ferroic orders as they enhance the number of properties and thus functionalities within the same system. Focusing on magnetic and ferroelectric orders, it is thus in principle possible in these materials to control magnetization using an electric field and conversely electric polarization with a magnetic field through magnetoelectric coupling. This particular topic has raised increasing interest in recent years [6–10], the research community enthusiasm being explained by the need for revealing the microscopic mechanisms behind the polarization–magnetization coupling as well as for practical application purposes. Such effect can be very attractive for instance for designing novel multifunctional devices within spintronics by limiting the detrimental and inherent Joule heating associated with the use of magnetic field in contrast with electric field [11,12].

Among multiferroics, $BiFeO_3$ (BFO) is the most widely considered compound because both polarization and magnetic orders coexist at room temperature [13,14]. Indeed, below the Curie temperature $T_C \sim 1100$ K [15,16], bulk BFO becomes ferroelectric, exhibiting a polarization value of $\sim 100\,°C/cm^2$ along the $\langle 111\rangle_C$ cubic-like directions [17]. The structure is described by the rhombohedral $R3c$ space group [18,19], which allows antiphase octahedral tilts and ionic displacements from the centrosymmetric positions about and along the same polar $[111]_C$ direction. Bulk BFO exhibits also a G-type antiferromagnetic order below the Néel temperature $T_N \sim 640$ K [20,21], where the Fe magnetic moments are coupled ferromagnetically within the pseudocubic $\{111\}_C$ planes and antiferromagnetically between first neighbors. An additional long-range spin cycloid modulation is superimposed on this antiferromagnetic order, resulting in a rotation of the spin axis through the crystal with a long period $\lambda \sim 62$ nm [22,23]. Because of the presence of this cycloid, magnetoelectric coupling arises from a quadratic term and remains weak [24,25]. When the cycloid is destroyed using a 20-T magnetic field, a small canting of the spin moments through the oxygen octahedra tilts gives rise to a weak magnetization, and a linear magnetoelectric coupling appears [26].

Interestingly, all these structural, polar and magnetic features are strain sensitive and thus BFO appears as a fantastic playground for strain engineering, where the strain can be exerted in a controlled manner in thin films through the differences in lattice parameters and thermal-expansion behaviors between the film and the underlying substrate. This strain engineering is now considered as a powerful means of tuning functionalities [27–29] and its emergence is explained by i) the maturity of epitaxial growth techniques with atomic control, in particular Pulsed Laser Deposition and Molecular Beam Epitaxy, ii) the easy availability of various high-quality substrates allowing a wide range of imposed misfit strain, iii) the high accuracy in predicting properties in films using state-of-the-art modeling tools, and iv) the desire to go towards ultrathin films and heterostructures with controlled properties in devices. A lot of progress has been made, especially in the case of the BFO system. Let us just mention here some of the difficulties the researchers have had to overcome when considering BFO films. Firstly, during BFO films growth, the high volatility of Bi should be considered to prevent any parasitic phase to appear. Secondly, the large number of degrees of freedom coexisting in BFO (polar mode, oxygen octahedra tilts, magnetic moment, effect of strain...) can easily make calculations a real nightmare. Furthermore, the weak structural distortions and the “heavy” and “light” atoms constituting BFO require an accurate and combined use of complementary techniques as synchrotron X-ray and neutron radiation facilities. Magnetic measurements are very challenging as any weak amount of impurities within the film and/or the substrate depicting paramagnetic or ferromagnetic signals can mask the response of the BFO film itself. Finally, in the case of dielectric and ferroelectric properties, the leakage is the main obstacle and requires particular attention. Despite all these difficulties, the efforts and ingenuity of researchers have succeeded to reveal some of the hidden and unexpected features of this multiferroic model system that we are going to present in the following.

2. Structure and phase transitions

The perovskite structure of BFO is rather singular, as both strong polar displacements (polarization of $\sim 100\ \mu C/cm^2$) and oxygen octahedra tilts (rhombohedral tilt angle of $\sim 13°$) coexist. These two degrees of freedom offer a plethora of possible symmetries for BFO (see Fig. 1) and also generate unexpected behaviors, as we shall see later on. Before describing the effect of epitaxial misfit strains on BFO films, let us first recall the complex situation in bulk BFO and the structures it can adopt. At ~ 1100 K, bulk BFO undergoes a first-order phase transition from its $R3c$ ferroelectric phase towards a high-temperature paraelectric phase that was experimentally ascribed as cubic $Pm\bar{3}m$ [30], orthorhombic-to-cubic $Pm\bar{3}m$ [31], rhombohedral $R\bar{3}c$ [32], monoclinic $P2_1/m$ [33], or orthorhombic $Pbnm$ [34] from different bulk forms and techniques (Raman spectroscopy, laboratory X-ray, synchrotron and/or neutron diffraction on single crystals, powders, and ceramics). Besides, results from first-principles calculations suggested a high-temperature transition towards indistinguishable rhombohedral $R\bar{3}c$ and cubic $Pm\bar{3}m$ phases [35] or to a phase depicting tetragonal $I4/mcm$ [36] or orthorhombic $Pnma$ [37] ($Pnma$ and $Pbnm$ are equivalent and just differ by their settings) space group. Today there is rather a consensus for claiming that this high-temperature phase should be orthorhombic. Nevertheless, the situation could be much more complicated than believed, as other exotic phases that are difficult to evidence experimentally despite some signatures have also been proposed. For all the above-mentioned space groups, except the cubic and rhombohedral ones, the phase transition is accompanied by both a loss of the center of symmetry and a change in the oxygen octahedra tilt system. As a matter of fact,

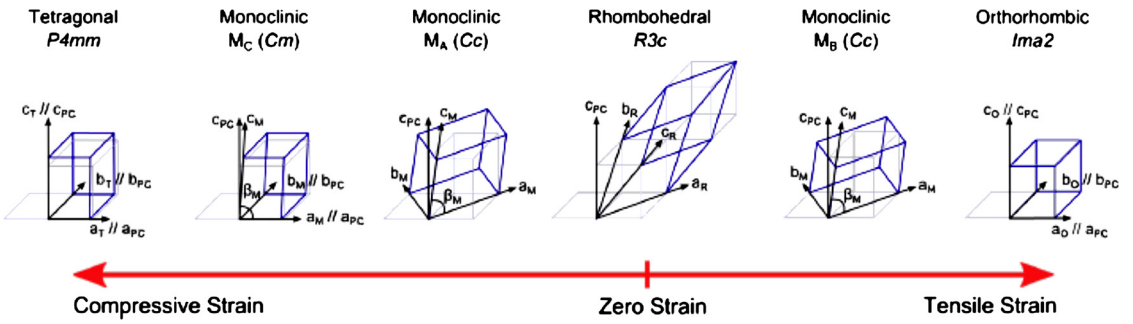

Fig. 1. (Color online.) Symmetry-strain dependence for epitaxial BFO thin films (from [14]).

the oxygen octahedra tilts existing within the rhombohedral phase may be seen as the primary order parameters driving this high temperature phase transition, thus BFO can be considered as a rather unusual improper ferroelectric [38]. Above ∼1200 K, another isosymmetric orthorhombic-to-orthorhombic phase transition has been proposed to be accompanied by an insulator-to-metal transition [39]; the latter was previously observed at room temperature under high hydrostatic pressure above ∼50 GPa [40]. Indeed, BFO is very sensitive to the application of an external pressure. Overall, above ∼10 GPa, the pressure stabilizes a *Pnma* orthorhombic phase at room temperature. Below this critical pressure of ∼10 GPa, several phases (orthorhombic and monoclinic) have been theoretically [41–43] and experimentally [44–48] reported to be stable, showing the pressure instabilities of the bulk BFO structure and presaging structural changes in BFO films, as typically the stress felt within the plane of growth within these epitaxial films can be of the order of several GPa.

Epitaxy refers to the continuation of a single crystalline thin layer (film) on top of a thick single crystal (substrate), with the particularity that ideally the in-plane lattice parameters of the film should coincide with those of the substrate [49]. When BFO film is deposited onto a substrate of another crystal formula, i.e. in case of a heteroepitaxial growth, there is a mismatch of the corresponding lattice parameters inducing a misfit strain on the film, which is technically forced to grow clamped onto the substrate surface. The strain energy usually accumulates rapidly when the film thickness increases until a critical thickness (of few tens of nanometers) where the strain energy is relaxed through formation of misfit edge dislocations, elastic domains, twins, etc. Depending on the conditions of growth and obviously on the strength of the misfit strain, the BFO films may be obtained fully strained. This latter situation typically corresponds to thicknesses smaller than 30–70 nm when grown along the $[001]_C$ cubic-like direction for a wide range of misfit strains. This critical thickness is unusually large and can be explained by the rather "flexibility" of BFO structure where both strong cationic shifts and oxygen octahedra tilts can absorb the epitaxial stress. The misfit strain is then strong enough to deviate the BFO structure from its bulk rhombohedral symmetry and even to induce novel highly distorted phases. For thicker BFO films, the structure starts to relax and tends towards the bulk-like rhombohedral symmetry.

Most of the available substrates allow the growth of BFO films along the $[001]_C$ cubic-like direction, typically on cubic $(001)_C$ or on the pseudocubic surface of crystals that are similar to $SrTiO_3$ (STO), like weakly rhombohedral ones such as $LaAlO_3$ (LAO) or orthorhombic ones as $DyScO_3$ (DSO) by taking the equivalence between (110)-orthorhombic and (001)-cubic planes. The possibility to explore a wide range of misfit strains from compressive (negative) to tensile (positive) on different materials [28,29] has been facilitated by the commercial availability of aluminate and scandate substrates like $YAlO_3$ (YAO), LAO, $(LaAlO_3)_{0.3}$–$(Sr_2AlTaO_6)_{0.7}$ (LSAT), DSO, $GdScO_3$ (GSO), $SmScO_3$ (SSO), $NdScO_3$ (NSO) or $PrScO_3$ (PSO) respectively imposing a misfit strain to BFO of $\sim -6.5\%$, -4.5%, -2.6%, -0.5%, -0.1%, $+0.2\%$, $+0.9\%$, $+1.2\%$. Note that active piezoelectric substrates like $Pb(Mg_{1/3}Nb_{2/3})O_3$–$PbTiO_3$ (PMN–PT) can be also used to tune the misfit strain in a more continuous way through the inverse piezoelectric effect by using an applied voltage on the substrate [50]. Bottom electrodes like $SrRuO_3$ (SRO), $La_{2/3}Sr_{1/3}MnO_3$ (LSMO) or $LaNiO_3$ (LNO) inserted in between the film and the substrate can allow electrical measurements while not strongly affecting the misfit strains and thus strain-related properties when growth is properly adapted to deposit BFO/electrode heterostructures. It is worth mentioning that, in the following, we will consider the film as a homogeneous object neglecting any additional effect due to the presence of strain gradients (or flexoelectricity), defects (impurities, dislocations, oxygen vacancies...), interfaces or roughness that should be taken into account for better describing the behavior of the film properties.

At room temperature and typically under moderate strain (see Fig. 1), say between -3% and $+2\%$, BFO adopts a monoclinic phase of space group *Cc* [51–54] which is the expected phase when the bulk *R*3*c* phase is clamped on a $(001)_C$ substrate [55–57], usually referred to as the R-phase. The *Cc* phase conserves the anti-phase oxygen octahedra rotation with a tilt system (*a*–*a*–*c*–) in Glazer's notation [58], while it is (*a*–*a*–*a*–) for the *R*3*c* space group. Pushing further the strain and towards larger values implies the removal of the oxygen octahedra tilts, thus the monoclinic *Cc* phase transforms into a *Cm* one while keeping the main feature of the monoclinic structures [56,59,60]. In detail, the symmetry of $\{011\}_C$ planes of these monoclinic phases allows the polarization vector to lie anywhere within one of these monoclinic planes and thus to rotate from the $[111]_C$ direction in the bulk rhombohedral unit cell either towards the $[001]_C$ direction by compression (tetragonal deformation, main polarization projection perpendicular to the film surface), which is usually referred to as M_A-type in that case, or towards the $[011]_C$ direction by tension (orthorhombic

deformation, main polarization projection lying within the film surface), which is typically referred to as M_B-type in that case [51,52,61,62]. This nomenclature was borrowed from the field of ferroelectrics and especially from the morphotropic phase boundary (MPB) in piezoelectric solid solutions [63,64]. These different monoclinic phases are also stable when BFO films are deposited following other growth directions [65,66], where the imposed anisotropic strain planes can facilitate stabilizing even triclinic phases [66]. Actually, such monoclinic *Cc* phase is also the one that bridges naturally the tetragonal and orthorhombic phases in most of the ferroelectrics in their temperature-misfit phase diagram, as the polarization vector can adjust itself easily to the substrate clamping. In this monoclinic phase of BFO, the c/a axial ratio that corresponds to the out-of-plane to in-plane lattice parameters ratio varies continuously with the misfit strain [67,68]. It increases roughly linearly under compressive strain until a critical misfit strain value of ∼4.5%, corresponding typically to BFO films deposited onto a LAO substrate where a consequent jump of the c/a ratio arises reaching unexpectedly high values of the order of 1.23 [67,69] (for comparison, the classical most distorted tetragonal $PbTiO_3$ ferroelectric has a c/a of ∼1.06 at room temperature). This jump marks the occurrence of a new phase having a strong tetragonality (high c/a ratio) that has been referred to as the T-phase or called the super-tetragonal phase.

The transition from R- to T-phase was first thought to be an isosymmetric *Cc*–*Cc* transition [55,57,70]. However, it was shown actually that the oxygen octahedra tilts disappear [56,60,71]. As a consequence, the only remaining structural way for the structure to relax is through an out-of-plane shift and thus a sudden enhancement of the c/a ratio is observed [56,67–69]. Therefore, alternatively, non-tilted space groups having close values in the energy landscape have been proposed, like the monoclinic *Cm* and *Pm* space groups as well as the pure *P*4*mm* tetragonal phase. The *Pm* symmetry is also referred to as M_C-phase in analogy with the MPB systems as it bridges the [001]-tetragonal phase and the [110]-orthorhombic phase through a {100}-cubic like plane. Note that a continuous cross from the $\{011\}_C$ planes of the M_A and M_B monoclinic phases to the $\{100\}_C$ plane of the M_C one requires triclinic phases that have also been reported in BFO films [72]. A pure tetragonal T-phase can be obtained for films with typical thickness of 10 nm and high enough misfit strain, for example using a YAO substrate [73]. This feature can be ascertained using piezoforce microscopy (PFM) measurements that demonstrate no lateral component of the polarization in contrast to *Pm* or *Cm* phases. Note that high misfit strain is not a necessary condition to get the T-phase and a buffer layer like β-Bi_2O_3 can be used to stabilize the super-tetragonal phase on a STO substrate [74] having a misfit strain of only $\sim -1.4\%$. Interestingly by playing on the growth conditions, the film thickness and the nature of the substrate, it is possible to obtain a coexistence of both R-phase and T-phase; such coexistence is investigated for getting enhanced electromechanical properties as in MPB systems. For instance, growing BFO on LAO and increasing the film thickness to release the strain favors such phase mixture [75]. It is worth recalling that R-like and T-like structures have very different c/a ratio and thus, to coexist, both structures should accommodate through misalignment with respect to the [001] perpendicular to the film direction and/or in-between phases with lower symmetry (triclinic phase) that can reduce the stored elastic energy.

The richness of the structures, the phase coexistence and associated functional properties are widely explored in the compressive misfit strain side of BFO films. In contrast, the tensile side is only poorly regarded, mainly because of the lack of appropriated substrates. An orthorhombic phase with an *mm*2 symmetry group has been revealed in 15-nm-thick BFO deposited onto NSO substrate, making the polarization vector lying in a ⟨011⟩ direction within the film plane [76]. An attempt to deposit BFO onto MgO has shown that BFO structure is rotated by 45° with respect to the substrate [77] to relax the huge nominal misfit strain ($\sim +6.6\%$). The structure is consistent with tilts of oxygen octahedra doubling the unit cell, and an orthorhombic with at maximum an *Fm*2*m* space group has been proposed. First-principles calculations have shown that indeed an orthorhombic phase is predicted under tensile strain. While an orthorhombic phase with an *Ima*2 space group was firstly predicted to occur at 0 K above $\sim +8\%$ misfit strain [78], another orthorhombic phase of lower energy with $Pmc2_1$ space group [79] has been suggested to emerge already above $\sim +5\%$. In both previous space groups, peculiar cation displacements combining in-phase and anti-phase polar shifts have been found, revealing unexpected features in BFO, including antiferroelectric-like behavior or charge ordering.

One may wonder now whether the various phase transitions of BFO are changed by the misfit strain as this latter strongly affects the structure. Temperature-driven phase transitions have been explored in both R-like and T-like phases. In the R-phase of fully strained or partially relaxed BFO films, the most remarkable finding concerns the unexpected decrease of the temperature T_C of the ferroelectric phase transition [68] when the strength of the misfit strain is increased (see Fig. 2). In classical ferroelectrics like the textbook examples $BaTiO_3$ and $PbTiO_3$, T_C increases with epitaxial strain. The experimentally observed decrease of T_C in BFO R-like films is understood by the interplay between polar shifts and oxygen octahedra tilts revealed by first-principles-based calculations [68]. Indeed, somehow the epitaxial stress is also absorbed by the octahedral tilts in contrast to classical ferroelectrics where only polar shifts play this role. Reciprocal space maps analysis have demonstrated that this phase transition takes place between a doubled monoclinic M_A-type phase and a primitive monoclinic one. At higher temperature, another phase transition towards a non-cubic phase has been also proposed [52]. While the critical ferroelectric point decreases with the misfit strain, that of the antiferromagnetic order, i.e. T_N, is only weakly changed [68]. Knowing that T_C is above T_N, then by increasing the strength of the misfit strain, one should make both critical points intercept and thus enhanced magnetoelectric coupling might be expected as both the dielectric and magnetic susceptibilities would diverge at the same temperature. Interestingly, in the T-phase when BFO is deposited on LAO, a structural phase transition occurs close to room temperature at ∼380 K, where both ferroelectric and magnetic transitions take place [80–82]. While the antiferromagnetic order clearly disappears, the exact ferroelectric nature of this

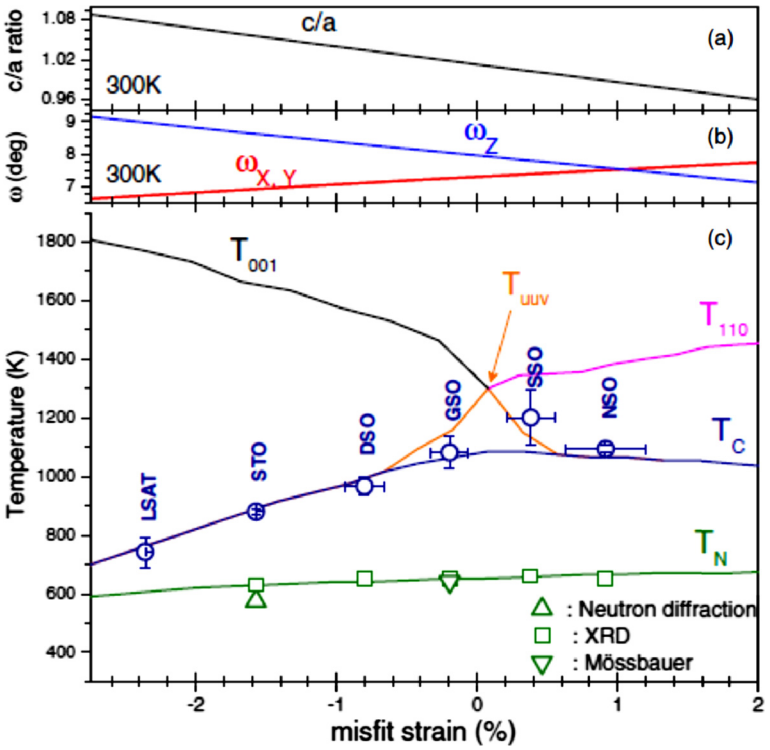

Fig. 2. (Color online.) Temperature versus misfit strain phase diagram for R-like BFO films (from [68]). Effective Hamiltonian evaluation at 300 K of (a) tetragonality (c/a ratio), and (b) antiferrodistortive angles ω along x, y, and z axes (ω_X and ω_Y, red line, and ω_Z, blue line). (c) Theoretical results on BFO film transition temperatures (T_C, blue line, and T_N, green line) as a function of misfit strain. The activation temperatures for the antiferrodistortive oxygen tilting along the z direction (tetragonal distortion T_{001}, black line), for the antiferrodistortive oxygen tilting within the x–y plane (orthorhombic distortion T_{110}, red line), and for the tilting along [uuv] direction (monoclinic distortion T_{uuv}, orange line) are also plotted. Experimental T_C (circles) and T_N (squares and triangles) values. Vertical error bars for T_N values correspond to symbol size and for T_C values result from maximum variation of T_C that may be obtained between different fitting processes using the mean field function. Below T_C, for any considered strain, the simulations predict that the crystallographic phase is Cc, with a polarization along a [uuv] direction while the oxygen octahedra rotate about a [$u_0u_0v_0$] axis.

above-380-K phase is not clear yet. Above 700 K, another structural transition is evidenced. This phase transition sequence for the T-phase has been proposed to correspond to a first-order transition from monoclinic M_C to monoclinic M_A phase and followed by a transition towards a pure tetragonal one [80]. In mixed R/T-phases samples, it looks that each phase evolves independently.

Beyond the most widely used (001) orientation we described previously, it is worth mentioning that (111) and (110) orientations using STO and DSO substrates, for instance, as well as unusual ones in between (110) and (001), giving rise to triclinic phases for BFO, have also been considered [83,66]. Besides, vicinal substrates like (001) STO crystal with few degrees of miscut have been also used [84,85]. Actually, the strategy here is much more related to the change and control of the morphology and size of the domains. Indeed, very recently the domain configuration and more especially the nature of the domain walls separating domains of two different polarization directions appear as an emerging field with a novel paradigm because the active element is the domain wall and not the domain itself. Indeed, the domain walls in BFO referred to as 71°, 109° and 180° (angles between the different domain variants in R-phase) have been suggested to be at the heart of the strong conductivity [86] or photovoltaic [87] behavior of BFO. While the intrinsic or extrinsic (defect-based) nature of these effects is not established yet [88], promising novel perspectives for BFO application are envisioned. An active research is thus currently underway and, while interesting, is out of the scope of this chapter. As we already mentioned, BFO is a ferroelectric. Thus, when it is deposited as a thin film, to avoid very large depolarizing fields which fight against the polarization perpendicular to the film surface in very thin films and to relax the epitaxial strain, for relatively thick film, the film tends to split into ferroelectric or ferroelastic domains, respectively. The scaling laws that relate the size of the domains with crystal thickness (Kittel's law for instance) are valid down to very low thickness, which implies that the size of the domains can be tuned down to a few nanometers by decreasing film thickness [89,85]. Actually, not only the size of the domains can be changed with thickness, but also the deposition on different miscut or type substrates, as well as with different electrical boundary conditions, has allowed controlling the type of domain walls present in the film as well as its morphology from fractal to stripe-like [90,91].

Based on the above description, it appears that the misfit strain strongly affects the structure and phase transition of BFO films. Therefore, it is legitimate to look now how the functional properties are in turn modified.

3. Polar properties of BFO thin films

The strategy of strain engineering in ferroelectrics is to enhance the out-of-plane polarization value [92]. Indeed stretching within the plane the unit cell, thanks to the substrate clamping, pushes upward the component of the polarization that is perpendicular to the plane. Therefore, one may expect a polarization value for BFO films higher than its bulk value, i.e. $\sim$100 μC/cm^2 along the [111] pseudo-cubic direction. However, in the R-type phase, whatever the growth direction is, i.e. along [001], [111] or [011], the polarization value projected along the [111]-cubic direction varies only weakly of about 15% (without mentioning the uncertainty of the measurement) with respect to the 100 μC/cm^2 bulk value [93–96]. Actually, in the R-phase, which is of *Cc* symmetry (i.e. monoclinic M_A- to M_B-type from compressive to tensile strain), the polarization vector is free to rotate within the monoclinic {011}-plane as similar to MPB systems. First-principles calculations have also demonstrated that suppressing the oxygen octahedra tilts makes the amplitude of the polarization increasing while the presence of the tilts favors rather the rotation of polarization vector without enhancement of its amplitude [54]. Therefore, once again, the interplay between polar shifts and oxygen octahedra rotations is revealed to be a key structural feature in BFO, as it is also responsible for the weak enhancement of the polarization value. When the tilts are turned off in the calculations, there is then a strong enhancement of the polarization as it reaches a value of $\sim$150 μC/cm^2. This value is reported experimentally for the so-called super-tetragonal T-phase [65].

The typical dielectric constant reported for bulk BFO is $\sim$40 at room temperature [97]. This rather low value can be partially explained by the fact that the ferroelectric phase transition takes place at high temperature ($T_C \sim 1100$ K). In the case of BFO thin films, dielectric constant measurements are scarce and typical values between $\sim$100 to $\sim$350 are reported at room temperature in the radiofrequency range [98–100]. It is not obvious to tell if such enhancement is due to the misfit strain, as the measurements are very difficult due to Maxwell–Wagner-like relaxations that arise from non-negligible conductivities at interfaces, defects, etc., which pollute the data. In order to improve the insulating properties of the films and limit the leakage current, doping BFO is the winning strategy. However, it affects also the other properties like magnetism and structure (for example [101]). This wide topic, i.e. doped-BFO and BFO-based solid solutions, is out-of-the scope of this chapter. Note finally that for microwave applications, a dielectric tunability (variation of the dielectric constant under electric field) of a few percent has been also reported in the GHz regime [102].

Interestingly, the piezoelectric properties (i.e., strain induced under applied electric field) that are reflected through the so-called d_{33}, which is the effective piezoelectric coefficient measured using PFM perpendicular to the film surface, appear to be much strain sensitive than the polarization. Indeed, in the R-phase, by varying the misfit strain by $\sim$3.5%, d_{33} increases from $\sim$20 pm/V to $\sim$50 pm/V, which corresponds to an enhancement of $\sim$250% [95]. These experimental values are in good agreement with theoretical predictions [57]. When the T-phase is reached, the d_{33} value remains of the same order and reaches about 30 pm/V [80]. Nevertheless, for mixed R/T phases, giant piezoelectric responses [67] are achieved with a d_{33} value of $\sim$120 pm/V and associated strains of the order of 2%, which are comparable or higher than for the best piezoelectric systems like PMN–PT. Such strong values are explained like in MPB system by the closeness of both R- and T-phase in the energy landscape. The external electric field can easily rotate the polarization vector from R-phase to T-phase and generate strong electromechanical properties. Domain re-distribution with domain wall displacements is also assumed to participate in this enhancement [103,104]. Searching for other equivalent MPB regions in the BFO system is also undertaken in the tensile side between the monoclinic and orthorhombic phase or also through the use of temperature-driven phase transitions or the use of solid solutions giving rise to other structural phases [105,106]. It is worth noting that, in BFO, strain can be induced by the application of an electric field, but also through light illumination via the so-called photostriction effect [107,108]. This topic is also currently under investigation.

4. Strain effect on magnetism in $BiFeO_3$ films

It is well known that two different magnetic structures have energies that are very close to each other in $BiFeO_3$ (BFO) bulk. As shown in, e.g. Refs. [17,22,23], the first structure is a magnetic cycloid that propagates in a plane spanned by the polarization (which lies along the pseudo-cubic $\langle 111\rangle_C$ directions) and the cycloid propagation direction (which is oriented along a second nearest-neighbor direction that is perpendicular to the polarization, such as the [1−10] direction). Such a structure has been proposed to originate from (i) Lifshitz-invariant energetic terms that are linear in electrical polarization and that involve the antiferromagnetic vector as well as its gradient [109–111], or (ii) from the (converse) spin–current model for which the corresponding energy is also linear in polarization and involves a cross-product between magnetic moments at different lattice sites [17,112–114]. These energies therefore predict that the formation of the magnetic cycloid is driven by the electrical polarization in BFO bulk. It is also worthwhile to realize that recent experimental and computational works [112,115] reported the occurrence of an out-of-plane spin density wave that is superimposed to the (in-plane) magnetic cycloid, therefore highlighting the complexity of the overall ground-state magnetic structure of BFO bulk. The second known magnetic structure is the so-called spin-canted state. It consists of a coexistence of a large G-type antiferromagnetic vector with a weak magnetization [116,117]. This weak magnetization originates from a Dzyalonshinskii–Moriya interaction involving the oxygen octahedral tilting (rather than the electrical polarization) [116–118].

Applying a physical factor to BFO bulk can lead to the transformation from one magnetic structure to the other [112]. For instance, an external magnetic field of around 20 T induces the transition from the magnetic cycloid to the (spin-canted)

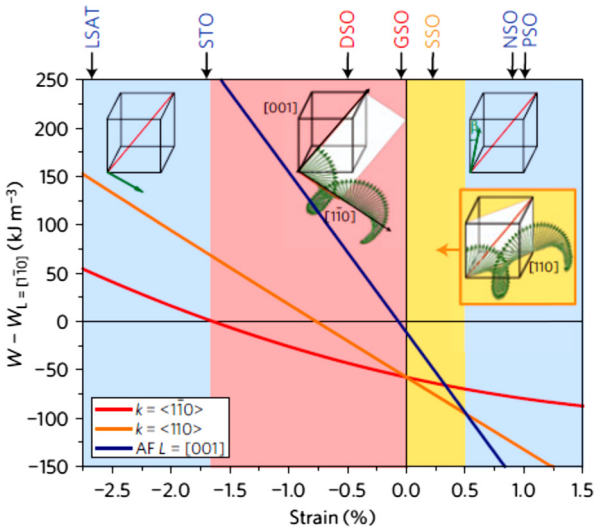

Fig. 3. Magnetic phase diagram of strained BFO films (from Ref. [120]). The energy of three magnetic states (bulk-like 'type-1' cycloid with propagation vector along [1$\bar{1}$0] directions, 'type-2' cycloid with propagation vector along [110] directions, and collinear antiferromagnetic order with antiferromagnetic vector close to [001]), relative to a fourth magnetic state, corresponding to a collinear antiferromagnetic order with antiferromagnetic vector along in-plane [1$\bar{1}$0] directions. The stability regions of the different states are shown in color (blue: antiferromagnetic; red: type-1 cycloid; orange: type-2 cycloid). The different substrates used i.e. $(LaAlO_3)_{0.3}$–$(Sr_2AlTaO_6)_{0.7}$ (LSAT), $SrTiO_3$ (STO), $DyScO_3$ (DSO), $GdScO_3$ (GSO), $SmScO_3$ (SSO), $NdScO_3$ (NSO) and $PrScO_3$ (PSO) are located on top of the diagram at their corresponding strain. Their color corresponds to the magnetic state determined from the Mössbauer measurements. The sketches represent the different magnetic states, with spins shown in green. For interpretation of the references to color, see the online version of this article.

G-type antiferromagnetism [119]. It is therefore legitimate to wonder what is the effect of epitaxial strain on the magnetic arrangements in BFO films.

To address this question, the authors of Ref. [120] grew (001) BFO films on top of different substrates, allowing the corresponding misfit strain to range between −2.6% (compressive strain) to +1.0% (tensile strain). Note that the corresponding structural state is the so-called R phase for this strain window. Using Mossbauer and Raman spectroscopies combined with Landau–Ginzburg theory and effective Hamiltonian calculations, it was found that (see Fig. 3), for compressive strains ranging between 0 and −1.5%, the aforementioned cycloid persists in the film. On the other hand, the magnetic ground state becomes the (spin-canted) G-type antiferromagnetic phase for compressive strains larger in magnitude than 1.5% and tensile strain larger than 0.5%. Interestingly, the direction of the antiferromagnetic structure was further discovered to rotate with the epitaxial strain from the in-plane [1$\bar{1}$0] direction at large compressive strain to the out-of-plane [001] direction at the largest investigated tensile strain. The resulting reorientation of spins was also proposed [120] to provide a handle for tuning exchange interactions with adjacent ferromagnets and spin valves. It should be noted that the fact that the antiferromagnetic vector was found (by Mössbauer spectroscopy, Landau–Ginzburg phenomenology, and effective Hamiltonian simulations) to lie along the [001] direction for large tensile strain in Ref. [120] contrasts with the results of another experiment [121] and some first-principles computations [78] reporting that the crystallographic direction of the antiferromagnetic vector is [1$\bar{1}$0]. Such difference emphasizes the difficulty of precisely extracting and measuring intrinsic properties of BFO films, as well as the unusual challenge that this material provides for theorists (as evidenced by, e.g., the fact that Diéguez et al. [37] demonstrated that several properties of BFO strongly depend on details of calculations, such as the choice of the functionality in the density-functional theory). Another controversial issue concerns the magnitude of the magnetization associated with the spin-canted structure in BFO films. For instance, it was predicted to be of the order of 0.03 Bohr magneton in Ref. [117] for BFO films grown on $SrTiO_3$ substrate. This is consistent with measurements of Refs. [122,123,13,124], but disagrees with the pioneering work of Ref. [125] (which led to the revival of multiferroics) that indicates that the magnetization can be as large as 1 Bohr magneton. Note that this large value of Ref. [125] was later suggested to be of extrinsic rather than intrinsic nature [122,123,13]. Furthermore, the authors of Ref. [120] also reported the unexpected existence of a novel type of magnetic cycloid in (001) BFO films when these latter are under a small tensile strain ranging between 0 and 0.5%. In this new type of cycloid, the magnetic moments rotate in a plane that still contains the electrical polarization and a propagation vector that is still along a second-nearest neighbor direction, but this latter is not perpendicular anymore to that polarization. For instance, the propagation can be along the pseudo-cubic [110] direction, while the polarization is close to lie along the pseudo-cubic [111] direction. It is also interesting to realize that the Néel temperature (at which magnetic ordering occurs) was mostly found to be insensitive to the misfit strain, and thus nearly always equal to 620–640 K, in Ref. [68], despite these magnetic rearrangements. Note also that the discovery of the new type of cycloid in (001) BFO films bears similarity with the prediction of Ref. [126] that BFO systems can indeed adopt different types of magnetic cycloid, but this latter prediction arises from the variation of the strength of the spin–current energetic interaction rather than from the change in magnitude and sign of the epitaxial strain.

As indicated above, all the aforementioned results about magnetic ordering in (001) BFO films pertain to the so-called R structural phase of these films. However, it is now well documented that BFO films can also adopt another type of crystallographic state, when the magnitude of the compressive strain is larger than around 4.5% (such strain corresponds to the growth of BFO on LAO substrates). This structural state is commonly termed the T-phase [67]. One may thus ask if such change in structure affects magnetic ordering and/or yields novel magnetic phenomena. The first-principles studies of Refs. [37,67,55,57,127] provided an answer to this question by predicting that the T-phase (when it is the ground state) typically and slightly energetically prefers, at low temperature, a C-type antiferromagnetic ordering rather than the G-type antiferromagnetic structure adopted by the R phase. Refs. [57,128] further indicated that the antiferromagnetic ground state of the T-phase is of G-type for smaller compressive strain and then becomes of C-type for compressive strains of the order of -5%, with further increasing the magnitude of the compressive strain stabilizing even more this C-type ordering (that is, it enlarges the difference in energy between the C-type and G-type antiferromagnetic structures). Interestingly, Escorihuela-Sayalero et al. [128] also predicted that a strong competition between magnetic interactions, and even magnetic frustration, should occur in the strain region around the G-to-C-type magnetic transition. Another interesting phenomenon for BFO films with similar strain is the observations and prediction that BFO grown on LAO undergo both a structural transformation and an antiferromagnetic-to-paramagnetic transition for temperatures around 340–370 K [80–82]. In other words, coupled ferroic transitions occur near room temperature! Another work conducted on BFO films grown on LAO also yielded technologically-promising results: He et al. [129] reported that these systems exhibit a structural organization at the nanoscale between R and T regions, with the R regions possessing a significant magnetization (about five times larger than those of films solely made of the R phase), which is further controllable by the application of an external electric field.

5. Magnetoelectric effect in $BiFeO_3$ systems

Magnetoelectric (ME) effects have been experimentally and theoretically investigated in $BiFeO_3$ bulks, as well as in films experiencing small misfit strains [17,112,117,57,24,25,36,130–133]. Typically, the ME effect is expressed as $P_i = \sum \alpha_{ij} H_j + \sum \beta_{ijk} H_j H_k$ or $M_i = \sum \alpha_{ij} E_j + \sum \gamma_{ijk} E_j E_k$, where P is the electric polarization, M is the magnetization, E and H are electric and magnetic field, α is the linear ME coefficient, and β and γ are two different quadratic ME coefficients. Interestingly, both linear ($\alpha = 4.1 \times 10^{-7}$ C/T m^2) and quadratic ME coefficients ($\beta = 1.9 \times 10^{-8}$ C/T^2 m^2) have been experimentally determined in $BiFeO_3$ systems [24,25]. More precisely, the quadratic, but not the linear, ME coefficient was found in BFO bulks under a magnetic field of less than 20 T. On the other hand, the linear ME coefficient was both reported in BFO bulks under a magnetic field larger than 20 T and in BFO films subjected to a large-enough epitaxial strain. The reason for this difference is related to the magnetic structure [26]: as indicated in the previous section, BFO bulks under magnetic fields smaller than 20 T exhibit a magnetic cycloid. Such a cycloid prevents the occurrence of the linear ME effect, but allows the existence of a non-vanishing β coefficient. On other hand, this magnetic cycloid is destroyed in favor of a spin-canted magnetic structure (possessing a weak ferromagnetism) in BFO bulks under larger magnetic field or in strained thin films made of BFO. This spin-canted structure can possess a linear magneto-electric coefficient, in addition to a quadratic one. Interestingly, the effective Hamiltonian-based work of Ref. [117] reveals that the weak magnetization inherent to the spin-canted structure (and which is induced by the tilting of oxygen octahedral) is essential for the linear ME effect to occur.

Another phenomenon related to magnetoelectricity is the ability to control the direction of the magnetic ordering by applying an electric field. Such an effect was indeed experimentally found in $BiFeO_3$ bulks [17,131] and thin films [132]. To understand it, let us recall that the magnetic cycloid of $BiFeO_3$ bulk propagates in the magnetic easy plane that is spanned by the polarization direction ($P \parallel [111]_{\text{pseudocubic}}$) and the cycloid propagation vector ($k \parallel [10\bar{1}]_{\text{pseudocubic}}$). As a result, applying an electric field that results in the change of the direction of the polarization by 71° or 109° automatically leads to the rotation of the easy plane of the magnetic cycloid [17,131]. Similarly, in thin films for which the spin-canted structure exists, the magnetic easy plane is inherently connected to structural features. For instance, this magnetic plane has first been proposed to be perpendicular to the electrical polarization [116] and perpendicular to the axis about which the oxygen octahedron tilts [134] (note that this latter axis is identical to the direction of the polarization in BFO systems under no strain and no electric field, but can be different if some misfit strain or electric field is applied). As a result, modifying these structural features (such as the direction of the polarization) by applying an electric field in BFO films can lead to a re-orientation of the magnetic order parameter. Moreover, using a combination of piezoelectric-force microscopy and X-ray photoelectron microscopy, Zhao et al. [132] have managed to simultaneously visualize the ferroelectric and antiferromagnetic domains, establishing that both types of domains are completely correlated with each other. Again, the easy magnetic plane can be changed by switching polarization under electric field by 71° and 109°, rather than by 180°.

The ME effects indicated above typically pertain to BFO systems under zero or relatively small strains. Let us now discuss ME effects under large compressive strain. Wojdeł et al. [57] and Prosandeev et al. [130] used two different but complementary ideas, resulting from the analysis of first-principles-based results, to tackle such issue. Wojdeł et al. [57] argued that structural softness can drive a giant ME effect, this softness being associated with materials in which the force-constant matrix (**K**) or elastic tensor (**C**) had vanishingly small eigenvalue for a soft mode. They found, by using a novel first-principles method to compute magneto-electric coefficients [135,136], that the linear ME coefficient (α) of the R-phase of BFO is enhanced (as compared to its zero-strain value) in the compressive strain ranging from -3% to -6%. Moreover, a very large α was indeed found, as a result of a very soft **K** eigenvalue, for a strain of -6%, at which the R-phase is a metastable state rather than the ground state (the T-phase is the ground state for that large strain). Moreover, Prosandeev

et al. [130] provided general analytical expressions of both the linear and quadratic ME coefficients in terms of polarization, as well as dielectric and magnetic susceptibilities, based on two different free-energy terms. Consistently with the work of Wojdeł et al. [57], both linear (α) and quadratic (β) ME coefficients were found to be enhanced under compressive strain, especially in the strain region for which the R-phase is a metastable state. This enhancement was explained by the increase in dielectric permittivity (which is expected if the material becomes soft). In other words, the two studies of Refs. [130] and [57] both predicted a strain-induced enhancement of magneto-electricity or electric-magnetism, with the explanations for their intrinsic origin being consistent with each other.

It is worthwhile to realize that a novel ME switching mechanism can also exist in strained BFO films. This was demonstrated in Ref. [133] where the authors studied the $Pmc2_1$ phase of BFO that has been predicted to occur at large tensile strains [79]. This phase is characterized by the existence of a polarization (**P**), an antiferroelectric vector (**A**), and an in-phase oxygen octahedral tilting ($\boldsymbol{\omega}$). Its magnetic structure consists of a primary G-type antiferromagnetic vector (**G**) that coexists with a secondary, weak A-type antiferromagnetic vector ($\mathbf{A}_{\mathrm{AFM}}$). Strikingly, two trilinear energetic terms, $\Delta E_1 = -C_1 PA\omega$ and $\Delta E_2 = -C_2\boldsymbol{\omega}\cdot(\mathbf{G}\times\mathbf{A}_{\mathrm{AFM}})$ where C_1 and C_2 are positive coefficients, were found in the $Pmc2_1$ phase of BFO [133]. The first energy term [118] implies that $\boldsymbol{\omega}$ can be switched by reversing **P** under an electric field (whereas it is difficult to switch **A** because of an associated large energy barrier). Moreover, the second energetic term implies that the switching of $\boldsymbol{\omega}$ naturally leads to the reversal of $\mathbf{A}_{\mathrm{AFM}}$ (whereas **G** is difficult to switch because of another large energy barrier). In other words, the magnetic order parameter ($\mathbf{A}_{\mathrm{AFM}}$ in this case) can be switched by electric field as a two-step process involving two original trilinear terms. This is also consistent with a recent work on superlattices made of $BiFeO_3$ and $LaFeO_3$ [137].

Let us also mention that other novel ME effects can occur too in BFO systems. For instance, a recent study predicted that applying curled electric fields in BFO nanodots can lead to a control of not only the magnitude, but also of the direction of the magnetization [138]. This phenomenon was termed “Magnetotoroidic effect”. Similarly, an even more recent work predicted that the chirality of the magnetic cycloid of BFO bulks can be switched by applying an electric field that is opposed to the initial polarization direction, via the existence of short-lived striking intermediate magnetic states [139] and as a consequence of the spin–current model. It was also predicted that applying an electric field can result in the transformation of the magnetic cycloid into the spin-canted structure, with the orientation of the weak ferromagnetic moment being controllable by the direction of the applied electric field [140]. Such an effect originates from a special kind of magnetic anisotropy that is linear in the applied electric field [140].

Interestingly, spin–wave frequency can also be influenced by the application of an electric field in $BiFeO_3$ because of linear magneto-electric effects, as nicely demonstrated in Refs. [110,141,142] on a theoretical level (based on a dynamical Ginzburg–Landau theory involving coupled magnetic and ferroelectric orders) and by measuring low-energy Raman scattering spectra. One remaining open question related to dynamical coupling between electric and magnetic degrees of freedom is whether the so-called electromagnons [143,144] exist or not in BFO. Different opinions have been expressed on such a question [141,145,146]. Finally, let us point out that, in our minds, studying and understanding how strain affects the cross-coupled electromagnetic susceptibility defined in Ref. [147] (and which characterizes the appearance of time-dependent magnetization when applying an ac electric field or, conversely, the occurrence of a time-dependent polarization under an ac magnetic field) is an interesting venue to explore in epitaxial BFO thin films in the near future.

Acknowledgement

This work is financially supported by ONR Grant N00014-12-1-1034 (Y.Y.), and NSF Grant DMR-1066158 (L.B.).

References

[1] G.A. Smolenskii, I.E. Chupis, Sov. Phys. Usp. 25 (1982) 475.
[2] H. Schmid, Ferroelectrics 162 (1994) 317.
[3] W. Eerenstein, N.D. Mathur, J.F. Scott, Nature 442 (2006) 759.
[4] Y. Tokura, J. Magn. Magn. Mater. 310 (2007) 1145.
[5] H. Schmid, J. Phys. Condens. Matter 20 (2008) 434201.
[6] N.A. Hill, J. Phys. Chem. B 104 (2000) 6694.
[7] M. Fiebig, J. Phys. D, Appl. Phys. 38 (2005) R123.
[8] S.-W. Cheong, M. Mostovoy, Nat. Mater. 6 (2007) 13.
[9] D. Khomskii, Physics 2 (2009) 20.
[10] L.W. Martin, R. Ramesh, Acta Mater. 60 (2012) 2449.
[11] C. Binek, B. Doudin, J. Phys. Condens. Matter 17 (2005) L39.
[12] M. Bibes, A. Barthélémy, Nat. Mater. 7 (2008) 425.
[13] G. Catalan, J.F. Scott, Adv. Mater. 21 (24) (2009) 2463–2485.
[14] D. Sando, A. Barthélémy, M. Bibes, J. Condens. Matter 26 (2014) 473201.
[15] Yu.E. Roginskaya, Yu.Ya. Tomashpol'skii, Yu.N. Venevtsev, V.M. Petrov, G.S. Zhdanov, Sov. Phys. JETP 23 (1966) 47.
[16] J.R. Teague, R. Gerson, W.J. James, Solid State Commun. 8 (1970) 1073.
[17] D. Lebeugle, D. Colson, A. Forget, M. Viret, A.M. Bataille, A. Gukasov, Phys. Rev. Lett. 100 (2008) 227602.
[18] C. Michel, J.-M. Moreau, G.D. Achenbach, R. Gerson, W.J. James, Solid State Commun. 7 (1969) 701.
[19] J.-M. Moreau, C. Michel, R. Gerson, W.J. James, J. Phys. Chem. Solids 32 (1970) 1315.
[20] S.V. Kiselev, R.P. Ozeron, G.S. Zhdanov, Sov. Phys. Dokl. 7 (1963) 742.
[21] V.G. Bhide, M.S. Multani, Solid State Commun. 3 (1965) 271.
[22] I. Sosnowska, T.P. Neumaier, E. Steichele, J. Phys. C, Solid State Phys. 15 (1982) 4835.

[23] I. Sosnowska, M. Loewenhaupt, W. David, R. Ibberson, Physica B, Condens. Matter 180 (1992) 117.
[24] C. Tabares Munoz, J.-P. Rivera, A. Bezinges, A. Monnier, H. Schmid, Jpn. J. Appl. Phys. 24 (1985) 1051.
[25] J.-P. Rivera, H. Schmid, Ferroelectrics 204 (1991) 23.
[26] Y.F. Popov, A. Zvezdin, G. Vorob'ev, A. Kadomtseva, V. Murashev, D. Rakov, D. Parsons, JETP Lett. 57 (1993) 69.
[27] D.G. Schlom, L.-Q. Chen, C.-C. Eom, K.M. Rabe, S.K. Streiffer, J.-M. Triscone, Annu. Rev. Mater. Res. 37 (2007) 589.
[28] D.G. Schlom, L.-Q. Chen, C.X. Pan, A. Schmehl, M.A. Zurbuchen, J. Am. Ceram. Soc. 91 (2008) 2429.
[29] D.G. Schlom, L.-Q. Chen, C.J. Fennie, V. Gopalan, D.A. Muller, X. Pan, R. Ramesh, R. Uecker, Mater. Res. Soc. Bull. 39 (2014) 118.
[30] R. Haumont, J. Kreisel, P. Bouvier, B. Dkhil, Phys. Rev. B 73 (2006) 132101.
[31] R. Palai, R.S. Katiyar, H. Schmid, P. Tissot, S.J. Clark, J. Robertson, S.A.T. Redfern, G. Catalan, J.F. Scott, Phys. Rev. B 77 (2008) 014110.
[32] S.M. Selbach, T. Tybell, M.-A. Einarsrud, T. Grande, Adv. Mater. 20 (2008) 3692.
[33] R. Haumont, I.A. Kornev, S. Lisenkov, L. Bellaiche, J. Kreisel, B. Dkhil, Phys. Rev. B 78 (2008) 134108.
[34] D.C. Arnold, K.S. Knight, F.D. Morrison, P. Lightfoot, Phys. Rev. Lett. 102 (2009) 027602.
[35] J.B. Neaton, C. Ederer, U.V. Waghmare, N.A. Spaldin, K.M. Rabe, Phys. Rev. B 71 (2005) 014113.
[36] I.A. Kornev, S. Lisenkov, R. Haumont, B. Dkhil, L. Bellaiche, Phys. Rev. Lett. 99 (2007) 227602.
[37] O. Diéguez, O.E. Gonzçalez-Vázquez, J.C. Wojdeł, J. Íñiguez, Phys. Rev. B 83 (2011) 094105.
[38] I.A. Kornev, L. Bellaiche, Phys. Rev. B 79 (2009) 100105.
[39] D.C. Arnold, K.S. Knight, G. Catalan, S.A.T. Redfern, J.F. Scott, P. Lightfoot, F.D. Morrisson, Adv. Funct. Mater. 20 (2010) 2116.
[40] A.G. Gavriliuk, V.V. Struzhkin, I.S. Lyubutin, S.G. Ovchinnikov, M.Y. Hu, P. Chow, Phys. Rev. B 77 (2008) 155112.
[41] P. Ravindran, R. Vidya, A. Kjekshus, H. Fjedllvåg, O. Eriksson, Phys. Rev. B 74 (2006) 224412.
[42] H.-J. Feng, F.-M. Liu, Chin. Phys. B 18 (2009) 1574.
[43] O.E. González-Vázquez, J. Íñiguez, Phys. Rev. B 79 (2009) 064102.
[44] R. Haumont, J. Kreisel, P. Bouvier, Phase Transit. 79 (2006) 1043.
[45] A.A. Belik, H. Yusa, N. Hirao, Y. Ohishi, E. Takayama-Muromachi, Chem. Mater. 21 (2009) 3400.
[46] R. Haumont, P. Bouvier, A. Pashkin, K. Rabia, S. Frank, B. Dkhil, W.A. Crichton, C.A. Kuntscher, J. Kreisel, Phys. Rev. B 79 (2009) 184110.
[47] D.P. Kozlenko, A.A. Belik, A.V. Belushkin, E.V. Lukin, W.G. Marshall, B.N. Savenko, E. Takayawa-Muromachi, Phys. Rev. B 84 (2011) 094108.
[48] M. Guennou, P. Bouvier, G.S. Chen, B. Dkhil, R. Haumont, G. Garbarino, J. Kreisel, Phys. Rev. B 84 (2011) 174107.
[49] M. Ohring, Materials Science of Thin Films: Deposition and Structure, 2nd edition, Academic Press, Harcourt Inc., San Diego, USA, 2001.
[50] E.J. Guo, K. Dörr, A. Herklotz, Appl. Phys. Lett. 101 (2012) 242908.
[51] G. Xu, H. Hiraka, G. Shirane, J. Li, J. Wang, D. Viehland, Appl. Phys. Lett. 86 (2005) 182905.
[52] H. Toupet, F. Le Marrec, C. Lichtensteiger, B. Dkhil, M.G. Karkut, Phys. Rev. B 81 (2010) 140101(R).
[53] C.J.M. Daumont, S. Farokhipoor, A. Ferri, J.C. Wojdeł, J. Íñiguez, B.J. Kooi, B. Noheda, Phys. Rev. B 81 (2010) 144115.
[54] H. Liu, K. Yao, P. Yang, Y. Du, Q. He, Y. Gu, X. Li, S. Wang, X. Zhou, J. Wang, Phys. Rev. B 82 (2010) 064108.
[55] A.J. Hatt, N.A. Spaldin, C. Ederer, Phys. Rev. B 81 (2010) 054109.
[56] B. Dupé, I.C. Infante, G. Geneste, P.-E. Janolin, M. Bibes, A. Barthélémy, S. Lisenkov, L. Bellaiche, S. Ravy, B. Dkhil, Phys. Rev. B 81 (2010) 144128.
[57] J.C. Wojdeł, J. Íñiguez, Phys. Rev. Lett. 105 (2010) 037208.
[58] A.M. Glazer, Acta Crystallogr., Sect. B, Struct. Crystallogr. Cryst. Chem. 28 (1972) 3384.
[59] F. Pailloux, M. Couillard, S. Fusil, F. Bruno, W. Saidi, V. Garcia, C. Carrétéro, E. Jacquet, M. Bibes, A. Barthélémy, G.A. Botton, J. Pacaud, Phys. Rev. B 89 (2014) 104106.
[60] Z. Chen, Z. Luo, C. Huang, Y. Qi, P. Yang, L. You, C. Hu, T. Wu, J. Wang, C. Gao, T. Sritharan, L. Chen, Adv. Funct. Mater. 21 (2011) 133.
[61] J.X. Zhang, Y.L. Li, Y. Wang, Z.K. Liu, L.Q. Chen, Y.H. Chu, F. Zavaliche, R. Ramesh, J. Appl. Phys. 101 (2007) 114105.
[62] H. Jang, S.H. Baek, D. Ortiz, C.M. Folkman, R.R. Das, Y.H. Chu, P. Shafer, J.X. Zhang, S. Choudhury, V. Vaithyanathan, Y.B. Chen, D.A. Felker, M.D. Biegalski, M.S. Rzchowski, X.Q. Pan, D.G. Schlom, L.Q. Chen, R. Ramesh, C.B. Eom, Phys. Rev. Lett. 101 (2008) 107602.
[63] D. Vanderbilt, M.H. Cohen, Phys. Rev. B 63 (2001) 094108.
[64] B. Noheda, Curr. Opin. Solid State Mater. Sci. 6 (2002) 27.
[65] G. Xu, J. Li, D. Viehland, Appl. Phys. Lett. 89 (2006) 222901.
[66] L. Yan, H. Cao, J. Li, D. Viehland, Appl. Phys. Lett. 94 (2009) 132901.
[67] R.J. Zeches, M.D. Rossell, J.X. Zhang, A.J. Hatt, Q. He, C.-H. Yang, A. Kumar, C.H. Wang, A. Melville, C. Adamo, G. Sheng, Y.-H. Chu, J.F. Ihlefeld, R. Erni, C. Ederer, V. Gopalan, L.Q. Chen, D.G. Schlom, N.A. Spaldin, L.W. Martin, R. Ramesh, Science 326 (2009) 977.
[68] I.C. Infante, S. Lisenkov, B. Dupé, M. Bibes, S. Fusil, E. Jacquet, G. Geneste, S. Petit, A. Courtial, J. Juraszek, L. Bellaiche, A. Barthélémy, B. Dkhil, Phys. Rev. Lett. 105 (2010) 057601.
[69] H. Béa, B. Dupé, S. Fusil, R. Mattana, E. Jacquet, B. Warot-Fonrose, F. Wilhelm, A. Rogalev, S. Petit, V. Cros, A. Anane, F. Petroff, K. Bouzehouane, G. Geneste, B. Dkhil, S. Lisenkov, I. Ponomareva, L. Bellaiche, M. Bibes, A. Barthélémy, Phys. Rev. Lett. 102 (2009) 217603.
[70] D. Mazumdar, V. Shelke, M. Iliev, S. Jesse, A. Kumar, S.V. Kalinin, A.P. Baddorf, A. Gupta, Nano Lett. 10 (2010) 2555.
[71] H.M. Christen, J.H. Nam, H.S. Kim, A.J. Hatt, N.A. Spaldin, Phys. Rev. B 83 (2011) 144107.
[72] Z. Chen, Y. Qi, L. You, P. Yang, C.W. Huang, J. Wang, T. Sritharan, L. Chen, Phys. Rev. B 88 (2013) 054114.
[73] H.J. Liu, H.J. Chen, W.I. Liang, C.W. Liang, H.Y. Lee, S.J. Lin, Y.H. Chu, J. Appl. Phys. 112 (2012) 052002.
[74] H.J. Liu, P. Yang, K. Yao, K.P. Ong, P. Wu, J. Wang, Adv. Funct. Mater. 22 (2012) 937.
[75] K.I. Doig, F. Aguesse, A.K. Axelsson, N.M. Alford, S. Nawaz, V.R. Palkar, S.P.P. Jones, R.D. Johnson, R.A. Synowicki, J. Lloyd-Hughes, Phys. Rev. B 88 (2013) 094425.
[76] J.C. Yang, Q. He, S.J. Suresha, C.Y. Kuo, C.Y. Peng, R.C. Haislmaier, M.A. Motyka, G. Sheng, C. Adamo, H.J. Lin, Z. Hu, L. Chang, L.H. Tjeng, E. Arenholz, N.J. Podraza, M. Bernhagen, R. Uecker, D.G. Schlom, V. Gopalan, L.Q. Chen, C.T. Chen, R. Ramesh, Y.H. Chu, Phys. Rev. Lett. 109 (2012) 247606.
[77] I.N. Leontyev, Yu.I. Yuzyuk, P.-E. Janolin, M. El-Marssi, D. Chernyshov, V. Dmitriev, Yu.I. Golovko, V.M. Mukhortov, B. Dkhil, J. Phys. Condens. Matter 23 (2011) 332201.
[78] B. Dupé, S. Prosandeev, G. Geneste, B. Dkhil, L. Bellaiche, Phys. Rev. Lett. 106 (2011) 237601.
[79] Y. Yang, W. Ren, M. Stengel, X.H. Yan, L. Bellaiche, Phys. Rev. Lett. 109 (2012) 057602.
[80] I.C. Infante, J. Juraszek, S. Fusil, B. Dupé, P. Gemeiner, O. Diéguez, F. Pailloux, S. Jouen, E. Jacquet, G. Geneste, Phys. Rev. Lett. 107 (23) (2011) 237601.
[81] J. Kreisel, P. Jadhav, O. Chaix-Pluchery, M. Varela, N. Dix, F. Sánchez, J. Fontcuberta, J. Phys. Condens. Matter 23 (34) (2011) 342202.
[82] W. Siemons, M.D. Biegalski, J.H. Nam, H.M. Christen, Appl. Phys. Express 4 (9) (2011) 095801.
[83] T. Shimada, K. Arisue, T. Kitamura, Phys. Lett. A 376 (2012) 3368.
[84] H.W. Jang, D. Ortiz, S.H. Baek, C.M. Folkman, R.R. Das, P. Shafer, Y. Chen, C.T. Nelson, X. Pan, R. Ramesh, C.B. Eom, Adv. Mater. 21 (2009) 817.
[85] C.M. Folkman, S.H. Baek, C.B. Eom, J. Mater. Res. 26 (2011) 2844.
[86] J. Seidel, L.W. Martin, Q. He, Q. Zhan, Y.H. Chu, A. Rother, M.E. Hawkridge, P. Maksymovych, P. Yu, M. Gajek, N. Balke, S.V. Kalinin, S. Gemming, F. Wang, G. Catalan, J.F. Scott, N.A. Spaldin, J. Orenstein, R. Ramesh, Nat. Mater. 8 (2009) 229.
[87] J. Seidel, D. Fu, S.Y. Yang, E. Alarcón-Lladó, J. Wu, R. Ramesh, J.W. Ager, Phys. Rev. Lett. 107 (2011) 126805.

[88] A. Bhatnagar, A.R. Chaudhuri, Y.H. Kim, D. Hesse, M. Alexe, Nat. Commun. 4 (2013) 2835.
[89] A. Schilling, T.B. Adams, R.M. Bowman, J.M. Gregg, G. Catalan, J.F. Scott, Phys. Rev. B 74 (2006) 024115.
[90] H. Béa, B. Ziegler, M. Bibes, A. Barthélémy, P. Paruch, J. Phys. Condens. Matter 23 (2011) 142201.
[91] B. Ziegler, K. Martens, T. Giamarchi, P. Paruch, Phys. Rev. Lett. 111 (2013) 247604.
[92] N.A. Pertsev, B. Dkhil, Appl. Phys. Lett. 93 (2008) 122903.
[93] H. Béa, M. Bibes, X.H. Zhu, S. Fusil, K. Bouzehouane, S. Petit, J. Kreisel, A. Barthélémy, Appl. Phys. Lett. 93 (2008) 072901.
[94] H. Jang, S.H. Baek, D. Ortiz, C.M. Folkman, R.R. Das, Y.H. Chu, P. Shafer, J.X. Zhang, S. Choudhury, V. Vaithyanathan, Y.B. Chen, D.A. Felker, M.D. Biegalski, M.S. Rzchowski, X.Q. Pan, D.G. Schlom, L.Q. Chen, R. Ramesh, C.B. Eom, Phys. Rev. Lett. 101 (2008) 107602.
[95] C. Daumont, W. Ren, I.C. Infante, S. Lisenkov, J. Allibe, C. Carrétéro, S. Fusil, E. Jacquet, T. Bouvet, F. Bouamrane, S. Prosandeev, G. Geneste, B. Dkhil, L. Bellaiche, A. Barthélémy, M. Bibes, J. Phys. Condens. Matter 24 (2012) 162202.
[96] M.D. Biegalski, D.H. Kim, S. Choudhury, L.Q. Chen, H.M. Christen, K. Dörr, Appl. Phys. Lett. 98 (2011) 142902.
[97] S. Kamba, D. Nuzhnyy, M. Savinov, J. Šebek, J. Petzelt, J. Prokleška, R. Haumont, J. Kreisel, Phys. Rev. B 75 (2007) 024403.
[98] X.Y. Zhang, X.C. Wang, F. Xu, Y.G. Ma, C.K. Ong, Rev. Sci. Instrum. 80 (2009) 114701.
[99] V.R. Palkar, J. John, R. Pinto, Appl. Phys. Lett. 80 (2002) 1628.
[100] K.-Y. Yun, M. Noda, M. Okuyama, H. Saeki, H. Tabata, K. Saito, J. Appl. Phys. 96 (2004) 3399.
[101] C.H. Yang, D. Kan, I. Takeuchi, V. Nagarajan, J. Seidel, Phys. Chem. Chem. Phys. 14 (2012) 15953.
[102] Faris B. Abdul Ahad, D.S. Hung, Y.D. Yao, S.F. Lee, C.S. Tu, T.H. Wang, Y.Y. Chen, Y.P. Fu, J. Appl. Phys. 105 (2009) 07D912.
[103] Z. Chen, S. Prosandeev, Z.L. Luo, W. Ren, Y. Qi, C.W. Huang, L. You, C. Gao, I.A. Kornev, T. Wu, J. Wang, P. Yang, T. Sritharan, L. Bellaiche, L. Chen, Phys. Rev. B 84 (2011) 094116.
[104] R.K. Vasudevan, M.B. Okatan, Y.Y. Liu, S. Jesse, J.C. Yang, W.I. Liang, Y.H. Chu, J.Y. Li, S.V. Kalinin, V. Nagarajan, Phys. Rev. B 88 (2013) 020402(R).
[105] H.J. Liu, C.W. Liang, W.I. Liang, H.J. Chen, J.C. Yang, C.Y. Peng, G.F. Wang, F.N. Chu, Y.C. Chen, H.Y. Lee, L. Chang, S.J. Lin, Y.H. Chu, Phys. Rev. B 85 (2012) 014104.
[106] C.W. Huang, Y.H. Chu, Z.H. Chen, J. Wang, T. Sritharan, Q. He, R. Ramesh, L. Chen, Appl. Phys. Lett. 97 (2010) 152901.
[107] B. Kundys, M. Viret, D. Colson, D.O. Kundys, Nat. Mater. 9 (2010) 803.
[108] M. Lejman, G. Vaudel, I.C. Infante, P. Gemeiner, V.E. Gusev, B. Dkhil, P. Ruello, Nat. Commun. 5 (2014) 4301.
[109] I. Sosnowska, A. Zvezdin, J. Magn. Magn. Mater. 140 (1995) 167–168.
[110] R. de Sousa, J.E. Moore, Appl. Phys. Lett. 92 (2) (2008) 022514.
[111] J. Jeong, E.A. Goremychkin, T. Guidi, K. Nakajima, G.S. Jeon, S.-A. Kim, S. Furukawa, Y.B. Kim, S. Lee, V. Kiryukhin, S.W. Cheong, J.-G. Park, Phys. Rev. Lett. 108 (7) (2012) 077202.
[112] D. Rahmedov, D. Wang, J. Íñiguez, L. Bellaiche, Phys. Rev. Lett. 109 (3) (2012) 037207.
[113] H. Katsura, N. Nagaosa, A.V. Balatsky, Phys. Rev. Lett. 95 (5) (2005) 057205.
[114] A. Raeliarijaona, S. Singh, H. Fu, L. Bellaiche, Phys. Rev. Lett. 110 (13) (2013) 137205.
[115] M. Ramazanoglu, M. Laver, I.W. Ratcliff, S. Watson, W. Chen, A. Jackson, K. Kothapalli, S. Lee, S.-W. Cheong, V. Kiryukhin, Phys. Rev. Lett. 107 (20) (2011) 207206.
[116] C. Ederer, N.A. Spaldin, Phys. Rev. B 71 (6) (2005) 060401.
[117] D. Albrecht, S. Lisenkov, W. Ren, D. Rahmedov, I.A. Kornev, L. Bellaiche, Phys. Rev. B 81 (14) (2010) 140401.
[118] L. Bellaiche, Z. Gui, I.A. Kornev, J. Phys. Condens. Matter 24 (31) (2012) 312201.
[119] D. Wardecki, R. Przeniosło, I. Sosnowska, Y. Skourski, M. Loewenhaupt, J. Phys. Soc. Jpn. 77 (10) (2008).
[120] D. Sando, A. Agbelele, D. Rahmedov, J. Liu, P. Rovillain, C. Toulouse, I.C. Infante, A. Pyatakov, S. Fusil, E. Jacquet, Nat. Mater. 12 (7) (2013) 641–646.
[121] M. Holcomb, L. Martin, A. Scholl, Q. He, P. Yu, C.-H. Yang, S. Yang, P.-A. Glans, M. Valvidares, M. Huijben, Phys. Rev. B 81 (13) (2010) 134406.
[122] H. Béa, M. Bibes, A. Barthélémy, K. Bouzehouane, E. Jacquet, A. Khodan, J.-P. Contour, S. Fusil, F. Wyczisk, A. Forget, Appl. Phys. Lett. 87 (7) (2005) 072508.
[123] H. Béa, M. Bibes, S. Petit, J. Kreisel, A. Barthélémy, Philos. Mag. Lett. 87 (3–4) (2007) 165–174.
[124] W. Eerenstein, F.D. Morrison, J. Dho, M.G. Blamire, J.F. Scott, N.D. Mathur, Science 307 (5713) (2005) 1203.
[125] J. Wang, J. Neaton, H. Zheng, V. Nagarajan, S. Ogale, B. Liu, D. Viehland, V. Vaithyanathan, D. Schlom, U. Waghmare, Science 299 (5613) (2003) 1719–1722.
[126] S. Bhattacharjee, D. Rahmedov, L. Bellaiche, D. Wang, MRS Commun. 3 (04) (2013) 213–218.
[127] Z. Chen, S. Prosandeev, Z. Luo, W. Ren, Y. Qi, C. Huang, L. You, C. Gao, I. Kornev, T. Wu, Phys. Rev. B 84 (9) (2011) 094116.
[128] C. Escorihuela-Sayalero, O. Diéguez, J. Íñiguez, Phys. Rev. Lett. 109 (24) (2012) 247202.
[129] Q. He, Y.-H. Chu, J. Heron, S. Yang, W. Liang, C. Kuo, H. Lin, P. Yu, C. Liang, R. Zeches, Nat. Commun. 2 (2011) 225.
[130] S. Prosandeev, I.A. Kornev, L. Bellaiche, Phys. Rev. B 83 (2) (2011) 020102.
[131] S. Lee, W. Ratcliff, S.-W. Cheong, V. Kiryukhin, Appl. Phys. Lett. 92 (19) (2008) 2906.
[132] T. Zhao, A. Scholl, F. Zavaliche, K. Lee, M. Barry, A. Doran, M. Cruz, Y. Chu, C. Ederer, N. Spaldin, Nat. Mater. 5 (10) (2006) 823.
[133] Y. Yang, J. Íñiguez, A.-J. Mao, L. Bellaiche, Phys. Rev. Lett. 112 (5) (2014) 057202.
[134] S. Lisenkov, D. Rahmedov, L. Bellaiche, Phys. Rev. Lett. 103 (4) (2009) 047204.
[135] J. Íñiguez, Phys. Rev. Lett. 101 (11) (2008) 117201.
[136] J.C. Wojdeł, J. Íñiguez, Phys. Rev. Lett. 103 (26) (2009) 267205.
[137] Z. Zanolli, J.C. Wojdeł, J. Íñiguez, P. Ghosez, Phys. Rev. B 88 (6) (2013) 060102.
[138] W. Ren, L. Bellaiche, Phys. Rev. Lett. 107 (12) (2011) 127202.
[139] S. Bhattacharjee, D. Rahmedov, D. Wang, J. Iniguez, L. Bellaiche, Phys. Rev. Lett. 112 (2014) 147601.
[140] R. de Sousa, M. Allen, M. Cazayous, Phys. Rev. Lett. 110 (26) (2013) 267202.
[141] M. Cazayous, Y. Gallais, A. Sacuto, R. De Sousa, D. Lebeugle, D. Colson, Phys. Rev. Lett. 101 (3) (2008) 037601.
[142] P. Rovillain, R. De Sousa, Y.t. Gallais, A. Sacuto, M. Méasson, D. Colson, A. Forget, M. Bibes, A. Barthélémy, M. Cazayous, Nat. Mater. 9 (12) (2010) 975–979.
[143] A. Sushkov, M. Mostovoy, R.V. Aguilar, S. Cheong, H. Drew, J. Phys. Condens. Matter 20 (43) (2008) 434210.
[144] R.V. Aguilar, M. Mostovoy, A. Sushkov, C. Zhang, Y. Choi, S. Cheong, H. Drew, Phys. Rev. Lett. 102 (4) (2009) 047203.
[145] G. Komandin, V. Torgashev, A. Volkov, O. Porodinkov, I. Spektor, A. Bush, Phys. Solid State 52 (4) (2010) 734–743.
[146] D. Wang, J. Weerasinghe, L. Bellaiche, Phys. Rev. Lett. 109 (6) (2012) 067203.
[147] K. Livesey, R. Stamps, Phys. Rev. B 81 (9) (2010) 094405.